Aerosol climate effects and air quality impacts from 1980 to 2030

Surabi Menon [1], Nadine Unger [2,3], Dorothy Koch[2,3], Jennifer Francis[4], Tim Garrett[5], Igor Sednev[1], Drew Shindell[2,3], David Streets[6]

[1] Lawrence Berkeley National Laboratory, Berkeley, CA, USA
[2] Columbia University, New York, NY, USA.
[3] NASA Goddard Institute for Space Studies, New York, NY, USA.
[4] Rutgers University, New Brunswick, NJ, USA
[5] University of Utah, Salt Lake City, UT, USA
[6] Argonne National Laboratory, Argonne, IL, USA

E-mail: smenon@lbl.gov

Abstract. We investigate aerosol effects on climate for 1980, 1995 (meant to reflect present-day) and 2030 using the NASA Goddard Institute for Space Studies climate model coupled to an on-line aerosol source and transport model with interactive oxidant and aerosol chemistry. Aerosols simulated include sulfates, organic matter (OM), black carbon (BC), sea-salt and dust and additionally, the amount of tropospheric ozone is calculated, allowing us to estimate both changes to air quality and climate for different time periods and emission amounts. We include both the direct aerosol effect and indirect aerosol effects for liquid-phase clouds. Future changes for the 2030 A1B scenario are examined, focusing on the Arctic and Asia, since changes are pronounced in these regions. Our results for the different time periods include both emission changes and physical climate changes. We find that the aerosol indirect effect (AIE) has a large impact on photochemical processing, decreasing ozone amount and ozone forcing, especially for the future (2030-1995). Ozone forcings increase from 0 to 0.12 Wm^{-2} and the total aerosol forcing increases from -0.10 Wm^{-2} to -0.94 Wm^{-2} (AIE increases from -0.13 to -0.68 Wm^{-2}) for 1995-1980 versus 2030-1995. Over the Arctic we find that compared to ozone and the direct aerosol effect, the AIE contributes the most to net radiative flux changes. The AIE, calculated for 1995-1980, is positive (1.0 Wm^{-2}), but the magnitude decreases (-0.3 Wm^{-2}) considerably for the future scenario. Over Asia, we evaluate the role of biofuel and transportation-based emissions (for BC and OM) via a scenario (2030A) that includes a projected increase (factor of two) in biofuel and transport-based emissions for 2030 A1B over Asia. Projected changes from present-day due to the 2030A emissions versus 2030 A1B are a factor of 4 decrease in summertime precipitation in Asia. Our results are sensitive to emissions used. Uncertainty in present-day emissions suggest that future climate projections warrant particular scrutiny.

Submitted to: *Env. Res. Let*

1. Introduction

To address the impacts of future climate, projections in the concentrations of both greenhouse gases (GHGs) and non-GHGs and their potential climate effects are important. The counteracting influence to GHG warming from the direct and indirect aerosol effects remains uncertain due in part to the complexity in treating aerosol-cloud interactions (Intergovernmental Panel on Climate Change 2007). Apart from the climate impacts of aerosols, changes to cloud and radiation fields from aerosols also affect the formation of ozone, which depends on the photooxidation of precursor emissions. Thus short-lived species such as aerosols and ozone are coupled, are both important for their climate and air quality impacts and have the potential to be important in near-term mitigation efforts.

The radiative forcing associated with ozone is $\sim$0.4 Wm^{-2} and for aerosols, forcings range from 0.3 (for black carbon (BC)) to -2.2 Wm^{-2} (for reflecting aerosols such as sulfates, organic matter (OM), nitrates and aerosol-cloud changes) based on emission changes from 1750 to present-day (PD) (Intergovernmental Panel on Climate Change 2007). Absorbing aerosols are thought to inhibit surface ozone formation by reducing the photolysis rates in polluted areas; whereas reflecting aerosols are thought to increase ozone formation (He & Carmichael 1999). Thus, future forcings depend on emission scenarios and relative changes in the distribution of precursors and reflecting versus absorbing aerosols (BC).

Here, we examine ozone and aerosol-cloud climate effects for three time periods: 1980, 1995 and 2030 using the NASA Goddard Institute for Space Studies (GISS) climate model (ModelE) coupled to an on-line aerosol chemistry/transport model. Aerosols simulated include sulfates, OM, BC, sea-salt and dust. The amount of tropospheric ozone is also calculated, thus allowing us to estimate both changes to air quality and climate for different time periods and emission amounts. Changes to future ozone forcing from coupling with an interactive sulfate chemistry model have been included in prior studies (Unger et al. 2006a, Unger et al. 2006b), however the addition of carbonaceous aerosols and their cloud impacts on future ozone forcing have not been included. Also, most prior studies of the aerosol indirect effects (AIE) focus on PD to pre-industrial (PI) time eras, and very few studies (e.g. Kloster et al. (2008)) account for changes in the AIE for future scenarios in simulations that include full couplings between the ozone and sulfate chemistry.

Since BC aerosols are more absorbing in the visible and due to their climate warming potential (Menon & Del Genio 2007), we single out their climate effects. We thus examine an alternative scenario with twice the 2030 A1B emissions from bio-fuel and transportation sources for OM and BC over Asia, due to the presence of a large proportion of these emissions over Asia (Fernandes et al. 2007) and a factor of two uncertainty in current residential emissions. Over India a large proportion of BC is from biofuel (Venkataraman et al. 2005); and the transportation sector over Asia is expected to grow with rapid economic expansion (Streets 2005). Furthermore, the transport of

Asian emissions to Arctic snow surfaces (Koch & Hansen 2005); and implied association between mid-latitude pollution and longwave cloud emissivity in the Arctic (Garrett & Zhao 2006, Lubin & Vogelmann 2006) suggest that these relevant issues should be examined for future changes. In section 2 we describe the methodology and model simulations; Section 3 includes the results from the simulations for both climate and air quality effects and the regional impacts of particulate matter (aerosols) and ozone for the Arctic and Asia. Finally in Section 4 the discussion and conclusions are presented.

2. Methodology

We use the GISS GCM (ModelE) (Schmidt et al. 2006) (4°x5° horizontal resolution and 20 vertical layers from 974 to 0.2 hPa) coupled to an on-line aerosol chemistry/transport model (Koch & Hansen 2005, Shindell et al. 2006, Koch et al. 2007a, Unger et al. 2006a) that includes schemes to treat the AIE (Menon et al. 2008, Menon & Del Genio 2007) and thus feedbacks between aerosols and clouds. We simulate the sulfur cycle and include source terms for OM and BC aerosols that are allowed to be transported and subject to the same physical processes (wet/dry deposition) as sulfates, but with reduced solubility. Both sea-salt and dust are treated as natural emissions. We use emissions for 1995 meant to reflect PD simulations and emissions for 1980 are used mainly to examine impacts over time periods where emission trends differ considerably across the developed and developing world. For future predictions, we confine our analysis to the 2030 A1B scenario since it represents a mid-range estimate of future growth in fossil-fuel emissions (other A1B aerosol projections may differ substantially (Shindell et al. 2007)). In this scenario, the atmospheric column burden for sulfates increase by 40% and the carbonaceous aerosols decrease by 16%. For the 1980, PD and 2030 simulations we use SST and sea-ice climatologies for 1975-1984, 1990-1999 and 2030-2039, respectively. Thus, both emission changes and climate effects are included and we do not separate between them. Unger et al. (2006b) found that climate and air pollution effects of emissions are more determined by emission changes for the 2030 A1B scenario than physical climate changes. Further details of the simulations and emissions used are in Appendix A.

We examine 3 sets of simulations for 1980, PD and 2030, shown in Table 1, listed as Sim 1980, Sim PD, Sim 2030, respectively, that include ozone-sulfate couplings, carbonaceous aerosols and the direct and indirect aerosol effects. Additional sensitivity tests include similar sets of simulations with only sulfates (OS) and without the AIE (listed as Sim 1980OS, Sim PDOS, and Sim 2030OS), and a simulation where bio-fuel and transportation sources of OM and BC are multiplied by 2 for Sim 2030 over Asia (10°S-40°N, 58°-122°E), described as Sim 2030A.

3. Results

Here, we present our analysis of changes in climate and air pollution due to the effects of ozone, aerosols and aerosol-cloud interactions as well as associated physical climate changes over the different time intervals we examine.

3.1. Aerosol and ozone distribution

To evaluate climate change for 1980 to 2030, we analyze the aerosol and ozone distributions for differences between PD and 1980 (referred to as "past") and for differences between 2030A1B and PD (referred to as "future"). Figure 1 shows annual surface concentrations for ozone (ppbv) and sulfate (μgm^{-3}). Past ozone concentrations increased overall over most parts of Asia and over Africa but decreased slightly over the US and Europe (similar to observed changes) in response to precursor emissions reductions legislation in these regions. Similar changes were found for sulfates described in more detail in Unger et al. (2006a) that performed similar analysis but without carbonaceous aerosols and the AIE.

Figures 2 and 3 show OM and BC surface concentrations (μgm^{-3}) for the past and future from both fossil, biofuel and biomass emissions. Similar to sulfate concentrations, the US and western Europe indicate a decrease in OM and BC emissions from fossil- and biofuel sources for the past, whereas emissions from these sources increased over parts of S. America, Africa, India and China. For biomass sources, increases (>2 μgm^{-3}, especially for OM) over Amazonia, southern parts of Africa, south-east Asia and Australia are noted for the past. For the past case the all-sky total (sulfate, BC and OM) aerosol optical depth (AOD) is 0.00. Both aerosol optical properties and mass distributions have been extensively evaluated with measurements, where available, and are described in Yu et al. (2006) and Koch et al. (2007b) in more detail. Additionally, AOD for Sim PD has been evaluated with satellite data for the Atlantic Ocean region (Menon et al. 2008). In general, the model tends to underestimate AOD, probably due to the assumed particle sizes and the underestimation of natural aerosols in southern tropical oceans (Koch et al. 2007b).

For the future case, mainly sulfates, ozone and biomass-based carbonaceous aerosols are projected to increase over Asia, while the Middle East shows an increase in fossil- and biofuel BC emissions (due to increased oil and gas extraction under the A1B scenario). The AOD for the future case is 0.02 (17% increase). While most emissions for sulfates, OM and BC decrease over the US and Europe, small ozone increases of the order of 2 ppbv are noted everywhere, which have been shown in a previous study to be largely due to future increases in methane since other short-lived precursor emissions decrease across the US and Europe for this scenario (Unger et al. 2006a). Differences between the ozone and sulfate concentrations for Sim 2030 versus Sim 2030OS are shown in Fig. 4. Globally, although the decrease for both ozone and sulfate are small, their distributions differ substantially. Ozone concentrations increase by a small amount over Europe and parts of China, eastern Australia and the Amazon, whereas, sulfate concentrations

increase over tropical ocean regions and SE Asia by over 10%. Asia, Europe and eastern US all show an increase of 5-8 %. Physical reasons for the differences are further discussed in the next sections where we consider cloud and radiation changes due to aerosols that could affect ozone formation and distribution, and sulfate precursors.

3.2. Aerosol and ozone forcings

For the aerosol and ozone distributions described above, we calculate the annual average instantaneous radiative forcings at the tropopause for aerosols and ozone for the past and future that are given in Table 2. Note that the differences between forcings for the different time periods also include changes from SSTs/sea-ice and GHGs in addition to differences in aerosol emissions. Given almost neutral changes in carbonaceous aerosols for the past case and the slight decrease in sulfate levels, the direct effect for the past case is close to 0.0 Wm^{-2}, and the larger increase in sulfate concentrations for the future results in higher negative forcings (-0.26 Wm^{-2}) since carbonaceous aerosols are almost constant. Table 3 indicates the forcing efficiency (radiative forcing/column burden) for the different aerosols we simulate that may be used to estimate the relative role that mitigation efforts may play in modulating aerosol distributions. BC from fossil- and biofuel sources clearly dominate forcing efficiency values and are almost a factor of 4 higher than sulfates and a factor of 10 higher than OM. Thus, for similar emission reductions, climate impacts from changes to BC distributions may play a larger role in mitigation studies than would impacts from changes to sulfates.

For ozone, we obtain forcings of 0.00 and 0.12 Wm^{-2} for the past and future cases. For the future case, forcings of 0.3 Wm^{-2} are found over tropical regions that have the high ozone concentrations, with decreases of up to -0.1 Wm^{-2} over the Arctic region, compared to the slight increase of 0.1 Wm^{-2} simulated for the past case. For simulations OS, ozone forcings are slightly higher for the past and future cases: 0.04 and 0.15 Wm^{-2}, respectively. Differences between simulations with the AIE and carbonaceous aerosols versus OS were found to be larger for the future case since the sulfate increase and the indirect effect is much more pronounced in the future scenario. The AIE may influence ozone chemistry through a number of pathways that change photolysis rates and wet deposition of precursors and thus ozone forcing. In general, for all of the three time periods analyzed, key photolysis rates increase by around 20% over the oceans and decrease by a few percent over land when carbonaceous aerosols and the AIE are included in the model versus the OS simulations (not shown). The increases in $J(O^1D)$ (photolysis of ozone to form O^1D) drive the reductions in surface ozone (Fig. 4) resulting in enhanced OH levels. OH increases by at least 5% across most mid-latitude regions and up to 20-30% at higher latitudes. The higher OH levels drive increases in gas-phase production of sulfate that result in higher surface concentrations across the northeastern US and Europe (Fig. 4). The sulfate increases in tropical regions shown in Fig. 4 are caused by increased aqueous-phase production for the simulation with the AIE and carbonaceous aerosols versus OS.

3.3. Aerosol-cloud interactions

The values for the AIE (calculated from changes to net cloud radiative forcing) for the past and future cases are -0.13 and -0.68 W m^{-2}, respectively, as shown in Table 2. Figure 5 shows the spatial distribution of cloud droplet number (CDNC), cloud optical depth (COD) and the AIE for the past and future cases. For past changes, the indirect effect is negative over land areas, but is positive over the South Asian subcontinent and SE Asia, parts of Africa and the northern US. These changes should be related to CDNC such that an increase in CDNC (and thereby a reduction in cloud droplet effective radii (R_{eff})) shoud generally coincide with areas of negative indirect effects, unless cloud liquid water and meteorology change. This is observed for the northern US and African regions. The increase in CDNC for the SE Asian region is due to the increase in carbonaceous aerosols, especially from biomass sources. However, the indirect effect was positive and the change in the sign of the AIE may be related to the decrease in cloud cover (CC) (not shown). Although CC (both total and low) increases globally for the past case (0.58%), these changes are not a result of the indirect effect as similar increases were also observed for simulations OS and may be related to climate feedbacks from imposed SSTs/sea-ice and GHG changes.

For the future case, similar to the increases observed for COD, the liquid water path (LWP) (not shown) indicates an increase of 2.36 gm^{-2}. Thus, the enhanced AIE for the future case is mainly due to the increase in LWP (at the expense of suppressed precipitation), and COD rather than CC. (Although physical climate changes may cause some of the increase in LWP or COD, compared to Sim (2030-PD), the increase in COD and LWP for Sim (2030OS-PDOS) are smaller by a factor of 1.6 and 20%, respectively, thus indicating an indirect effect signal). In terms of the distribution of the AIE impacts, for future changes the average AIE over the NH land areas is 0.61 Wm^{-2} compared to -1.49 Wm^{-2} found for the SH land areas, indicative of the effects of decreased aerosol emissions (especially sulfates) over most mid-latitude land areas. AIE values over land and ocean are 0.03 and -0.89 Wm^{-2}, respectively, indicating where the response is likely to shift with a change in emissions.

3.4. Impacts of the aerosol indirect effect on ozone forcing

The impact of the AIE and carbonaceous aerosols on the annual average ($J(O^1D)$) and ($J(NO_2)$) photolysis rates at the surface for the future case given as Sim (2030-PD) - Sim (2030OS-PDOS) is shown in Fig. 6. Photochemistry is suppressed in subtropical and tropical regions where COD has increased due to the increased aerosol loading between 2030 and 1995 (Fig. 5) resulting in a dampening of the global ozone increase for the future case. The inclusion of the AIE may also impact other processes that affect ozone, especially wet deposition. Figure 7 shows the impact of the AIE on the change of rate of wet deposition of nitric acid (HNO_3) between 2030 and 1995 [(2030-PD) - (2030OS-PDOS)]. Similar effects are expected for other wet deposited species. It is evident that the spatial pattern of the changes follows the changes in CDNC and LWP/COD for

the time period (e.g. Fig. 5). Where precipitation decreases in subtropical regions due to increases in aerosol loading, the wet deposition of ozone precursors is reduced relative to the OS simulations. Conversely, in some NH mid-latitude regions where aerosols have been reduced, especially the northeastern US, the opposite effect (not desirable for reducing acid deposition) is apparent. A decreased in wet deposition of ozone precursors would tend to increase ozone amounts in the troposphere. However, the decrease in surface ozone found in Fig. 4 suggest that the influence of aerosol-cloud interactions on wet deposition must be outweighed by the influence on photolysis rates.

3.5. Regional Impacts

Due to the heterogeneity in aerosol emissions, we evaluate regional changes over two areas of interest: the Arctic (60°-90°N) and Asia (10°S-40°N, 58°-122°E). These regions are chosen to analyze the influence of short-lived pollutants (aerosols and ozone) on the Arctic surface radiation (given the sensitivity of high latitude regions to future climate change) and changes to precipitation and air quality from aerosols and ozone over the Asian monsoon region.

3.5.1. Aerosol and ozone impacts on the Arctic climate To understand the relative influence of aerosol emissions on the distant Arctic climate we examine the annual values of radiative fluxes, cloud cover and temperature over the Arctic region and include seasonality since Arctic summer versus winter clouds have different distributions of liquid versus solid-phase clouds. Note that our simulations include physical climate changes in addition to aerosol changes and thus radiative forcing differences are actually flux differences. Our simulations do not include impacts of aerosols on cold cloud processes, via changes to ice nuclei. Thus changes we identify are a result of feedbacks associated with aerosol direct radiative effects and aerosol impacts on liquid-phase clouds, whenever they exist. Table 4 lists the annual, summer and winter averages for several variables (radiation and cloud fields) for the three time periods. We find an increase in surface radiation, TOA net radiation and a decrease in low and total CC for the future case compared to the past. The indirect effect decreases (more negative) for the future case. As expected during winter LWCRF dominates the net cloud radiative forcing giving us a net positive indirect effect though the magnitude gets weaker for the future. Although the low and total cloud cover decrease, liquid-phase cloud cover increases for the future case (at the expense of a decrease in the ice-phase clouds) and surface air temperature (SAT) decreases. Projected changes in ozone forcing for the Arctic are small and decreases for the future (goes from 0.03 to -0.02 Wm^{-2}). The aerosol direct forcing values in Table 4 are also rather small. Given such a large change in the AIE, from 1.0 to -0.30 Wm^{-2} (from the past to the future), we compare some of the simulated cloud microphysical values for Sim PD with available measurements over the Arctic (Barrow region), to constrain the contribution of the indirect effect to Arctic surface radiative changes, in Appendix B.

As shown in Appendix B, while R_{eff} and COD are within retrieval uncertainties as given in Zhao & Garrett (2008), larger/smaller values are simulated for CDNC and LWP that are not within retrieval uncertainties. However, radiative fluxes are more sensitive to both R_{eff} and COD and thus due to compensating biases in CDNC and LWP, simulated radiative fluxes may be a useful indicator of future changes. Since downwelling longwave fluxes (DLW) are expected to contribute most to the Arctic surface radiation balance (Francis & Hunter 2007, Garrett & Zhao 2006), we examine DLW fluxes obtained from the television and infrared observation satellite operational vertical sounder (TOVS) instrument (Francis 1997) and compare them to simulated DLW fluxes. These DLW fluxes are sensitive to cloud fraction, cloud droplet size, and cloud water paths and thus provide a measure of the relative impacts of clouds on the surface radiative flux. Global annual averages of DLW fluxes decrease from 1980 to 2030 but increase for the Arctic region. Annual average DLW fluxes over the Arctic surface retrieved from TOVS for 1980 to 2004 are shown in Fig. 8. Similar values from Sim 1980, PD and 2030 are 228.7, 232.5 and 235.9 Wm^{-2}, respectively. Both observations and simulations indicate a slight increase in DLW fluxes (<5%). Simulated fluxes are within retrieval uncertainties, that are rather large, but are lower than average values for the Arctic region by $\sim$ 10%, and by 5 to 10% for Barrow (Appendix B).

An increase in DLW fluxes could imply reduced cloud cover and increased SAT as shown in Table 5. However, although June to August SAT values increase for the future case, annual SAT decreases. Using a similar model, Shindell (2007) finds that SAT response may be more coupled to remote forcings than local forcings and can show an opposite response to local forcings. Thus, SAT response may be more dominated by non-aerosol forcings.

3.5.2. Climate impacts from increase in transportation and bio-fuel based carbonaceous emissions over Asia For the future scenario considered here, carbonaceous aerosols are projected to decline over most parts of the globe, including Asia, where concentrations are generally high. Koch et al. (2007b) finds that PD carbonaceous aerosols over Asia may be lower than observed amounts which may in part be due to emission sources used (Cao et al. 2006). Thus, it is quite likely that the sensitivity test (Sim 2030A) we carry out, where carbonaceous aerosols (OM and BC) from biofuel and transportation sources for 2030 A1B increase by 2x over Asia (10°S-40°N and 58°E-122°E), may not be unrealistic.

We examine the differences in aerosol and ozone forcings for this region for the future case as shown in Table 5. Globally, average values for the ozone and the total aerosol forcing (direct+indirect) are 0.12 and -0.94 (-0.26 + -0.68) Wm^{-2}, respectively, while over the Asian region considered here, average values for ozone and the total aerosol forcing are 0.23 and -0.86 (-0.50 + -0.36) Wm^{-2}, respectively. Thus, Asian averages are about twice the global averages for ozone and the direct effect and almost half the global value for the AIE. For Sim 2030A, ozone forcing increases by 9% and the total aerosol forcing decreases by 75% mainly due to the decrease in the indirect effect

(decrease in low CC and LWP probably due to the heating effects of BC aerosols), as shown in Table 5. The indirect effect thus increases from -0.36 Wm^{-2} to 0.27 Wm^{-2}. With the increased carbonaceous emissions, apart from the large increase in submicron aerosol mass, net TOA radiation decreases by 30%, implying a less reflective atmosphere and a warmer surface, with an increase in surface ozone and particulate mass.

Precipitation changes for June to August are shown in Fig. 9 for the past and future cases. The increase in summer precipitation over southern China, similar to that found in Menon et al. (2002), and large parts of SE Asia for the past case is reduced for the future cases. Similar changes are observed for the eastern and western parts of India. These changes in precipitation are due to both emission and physical climate changes. The impact of the increase in carbonaceous aerosol emissions on precipitation for the Asian region studied here are a factor of 4 decrease for Sim (2030A-PD) versus Sim (2030-PD), shown in Fig. 9. Thus, increases in biofuel and transport-based carbonaceous emissions result in a reduction in average precipitation, with some regions (e.g. northern China and eastern India) indicating an increase in precipitation. Similar spatial redistributions in precipitation due to the heating effects of Asian haze were found by Chung & Ramanathan (2006) and Ramanathan et al. (2005) for the South Asian region.

Since Koch & Hansen (2005) found that Asian emissions may impact the distant Arctic we evaluate similar diagnostics as shown in Table 4 for Sim 2030A-PD, but for annual differences only. We find that values for the aerosol direct forcing (-0.03 Wm^{-2}) and ozone forcing (0.00 Wm^{-2}) are negligible. The indirect effect (-0.51 Wm^{-2}) and values for net radiation both at the surface (1.39 Wm^{-2}) and TOA (0.37 Wm^{-2}) are larger than that found for Sim 2030-PD, mainly due to changes in LCC (-0.95) and WCC (-0.45). Thus, the bigger impact from increased carbonaceous emissions over Asia is in the aerosol indirect effect (mainly from cloud changes).

4. Discussion and conclusions

We use a series of model simulations, for 1980, 1995 (PD) and 2030, to estimate changes in aerosol and ozone forcing, both globally and across two regions of interest - the Arctic and Asia. Simulated climate include effects from both changing emissions and a changing climate (from changes in SSTs/sea-ice and GHGs).

With a projected increase in sulfate emissions and a slight reduction in carbonaceous aerosols for 2030, the aerosol forcing (both the direct and indirect effects) decreases from -0.10 (for PD versus 1980) to -0.94 (for 2030 versus PD) Wm^{-2}. Similar changes for the ozone forcing are an increase from 0 to 0.12 Wm^{-2} due to an increase in ozone precursors. Differences between simulations with carbonaceous aerosols and the AIE versus simulations with just sulfate aerosol direct effects are a small decrease in surface sulfate and ozone with larger changes in surface sulfate over tropical regions. Globally, ozone forcing decreases between 2030 and 1995 relative to simulations with just sulfates. The ozone reductions appear to be driven by a reduction in photolysis due to increased

cloud optical depth in the subtropics as a result of the enhanced aerosol loading there.

Over the Arctic, the AIE dominates the ozone and direct aerosol forcing, with positive values of the indirect effect of +1 Wm^{-2}, calculated for PD-1980, changing to negative values of -0.3 Wm^{-2} for the future case (2030 - PD). Since the AIE was only applied to liquid-phase clouds, model simulated cloud microphysical properties and radiative fluxes for PD were compared to available measurements for the summer season when shallow liquid-phase stratus clouds persist in the Arctic. Simulated cloud droplet size and optical thickness are comparable to retrieved values, however, cloud droplet number and LWP were over and under-predicted. Since radiative fluxes are more sensitive to cloud optical depth and droplet size, simulated downwelling LW fluxes were comparable to retrieved values. Both total and low level clouds decrease in the future scenario, and thus the downwelling LW flux and net surface radiation increase. However, the surface temperature decreases, which may be subject more to large-scale dynamical changes than to the aerosol forcing.

Over Asia, both ozone and the aerosol direct effect are twice the global averages, while the AIE is half of the global average. With the expected increase in transportation over Asia and the larger proportion of global biofuel used in Asia, we carried out a sensitivity test (Sim 2030A) with twice the biofuel and transport-based emissions from carbonaceous aerosols for Asia for the 2030 A1B scenario. Resulting changes are a 9% increase in ozone forcing, a 75% reduction in the aerosol forcing and a factor of four decrease in precipitation for 2030A-PD versus 2030-PD. Impacts on the distant Arctic due to the increased Asian emissions are mostly evident in the indirect aerosol effect (from cloud changes).

Our results are sensitive to the change in physical climate from GHG and SSTs/sea-ice changes and projected emissions of reflecting versus absorbing aerosols. Since prior work by Unger et al. (2006b) indicated that climate effects are more sensitive to emission changes than physical climate changes for the future scenario considered here, uncertainties in aerosol emissions or precursors would necessarily result in uncertain climate projections. Given the large aerosol forcing values we obtain and the uncertainty in indirect effect simulations, the PD simulations used in this paper were compared to satellite retrievals and meteorological data for June to August 2002 over the Atlantic Ocean to constrain the magnitude of the indirect effect (Menon et al. 2008). Results suggest that our PD simulations may slightly over-predict the indirect effect over the Atlantic Ocean region and thus our AIE estimate may be considered an upper limit for expected changes. Relatively few studies account for the impacts of the AIE on tropospheric ozone. Our analysis suggests large potential impacts on photochemical processing and thus the aerosol-cloud interactions need to be included in simulations of past and future ozone changes. In future work we will explore the impacts of the AIE on ozone production and loss mechanisms in different regions for past and future changes.

Acknowledgments

This research was supported by the NASA MAP and Radiation Sciences Programs; the DOE Atmospheric Radiation Program; and the DOE Intergrated Assessment Program. This work was supported by the Director, Office of Science, Office of Basic Energy Sciences, of the U.S. Department of Energy under Contract No. DE-AC02-05CH11231.

Appendix

A: Description of simulations and emissions

Monthly mean sea surface temperatures (SSTs) and sea ice cover are prescribed to 1975-1984 values for the past simulations (Rayner et al. 2000). For the present and future simulations (1990-1999 and 2030-2039) monthly mean SSTs and sea ice cover are prescribed to values that were generated in a previous simulation of the GISS atmosphere-ocean model (Russell et al. 2003). The changes in surface temperatures associated with the changing SSTs/sea-ice we include are 0.63 K for the past (PD-1980) and 0.69 K for the future (2030-PD) (see Fig.2 of Unger et al. (2006a)).

Methane concentrations are prescribed to values that were generated in previous simulations with a similar model but using a fully interactive methane cycle including climate sensitive emissions from wetlands (Unger et al. 2006b). In the PD simulations methane concentrations are 1802 ppbv in the northern hemisphere and 1655 ppbv in the southern hemisphere. For the 2030 A1B atmosphere human-made methane emissions increase by 75% relative to 1995, which lead to concentration projections of 2603 ppbv in the northern hemisphere and 2353 ppbv in the southern hemisphere. For the 1980 simulations, methane concentrations are fixed to observations for that period (1690 ppbv in the northern hemisphere and 1560 in the southern hemisphere). GHG levels for the three time periods are set to values at 1980, 1990 and 2030 (Hansen et al. 2005). Chemical fields are calculated in the troposphere only, with stratospheric ozone and other species prescribed according to observations (Shindell et al. 2006).

Present-day aerosol emissions are those used in Koch et al. (2007b) and the 2030 A1B emissions are those used in Koch et al. (2007a) based on Streets et al. (2004). The 1980 emissions are from Streets et al. (2006). Biomass burning for the past and future are based on projected changes (Streets et al. 2004, Streets et al. 2006) applied to the GFED emissions v1, 1997-2001, also described in Koch et al. (2007b) (from e.g. van der Werf et al. (2004)) together with the carbonaceous aerosol emission factors from Andreae & Merlet (2001).

Aerosols are externally mixed and to convert aerosol mass to aerosol number we use assumed log-normal size distributions as specified in Menon & Rotstayn (2006). Although the model resolution is coarse the tracers are advected with a highly nondiffusive quadratic upstream scheme that increases the effective resolution of the tracer fields. The aerosol-cloud interactions we simulate for liquid-phase stratus and cumulus clouds, include (a) the first AIE: increased (decreased) cloud reflectivity due

to an increase (decrease) in aerosols and cloud droplet number concentrations (CDNC) and reduced (increased) droplet sizes (R_{eff} for similar cloud liquid water content (LWC) (Twomey 1991); and (b) the second AIE: change in cloud cover (CC), cloud liquid water path (LWP) and precipitation due to smaller droplet sizes that inhibit precipitation processes, thereby increasing CC and LWP (and thu s cloud optical depths (COD)) (Albrecht 1989). Aerosols that can impact cloud processes via CDNC include sulfates, OM, BC and sea-salt.

Aerosol radiative forcing is obtained from the difference in the radiative flux with and without aerosols calculated at each model timestep at the tropopause. Our aerosol indirect effect is calculated from differences in the total and clear-sky net TOA radiative flux (SW + LW) at each model timestep. This is thus the cloudy sky radiative flux and differences between sets of simulations includes the cloudy sky forcing changes and other feedbacks. Since we allow for cloud changes, the definition does not follow that of the Intergovernmental Panel on Climate Change (2007) as also stated in Kloster et al. (2008). Model simulations are run for 6 years (equilibrium simulations) and averages for the last 5 years are given, allowing for sufficient spin-up time. Although statistical significance of the results are not shown, in general, most results, above the minimum difference indicated by the white bar in the figures, are significant at the 95% level based on a student's t-test, as also shown in Bell et al. (2005), and based on similar simulations with a similar version of the model.

B: Comparing simulated cloud microphysical properties with observed data from the Arctic

Ground-based remote sensing measurements for single-layer Arctic stratus clouds using data from the Atmospheric Radiation Measurement Program's site at the North Slope of Alaska (Barrow region) are available for 2000 to 2003 (Zhao & Garrett 2008) for single-layer clouds with bases below 4 km, COD ≤ 8 and $R_{eff} \leq 25$ μm. Climatological ranges of cloud properties for June to August (maximum occurrence of liquid-phase clouds) for all single-layer thin clouds of thickness between 300 to 1200 m are 10 to 12 μm and 20 to 40 cm^{-3} for R_{eff} and CDNC, respectively. Values of 3.5 to 4.5 and $\sim$ 30 gm^{-2} were obtained for COD and LWP, respectively. Retrieval uncertainties for the 95% confidence level for R_{eff}, CDNC, COD and LWP are 7%, 30%, 15% and 10%, respectively. Although ground-based measurements cannot easily be compared with values from a coarse grid model, the general characteristics may be compared to evaluate basic features simulated by Sim PD. We use daily data for similar time periods (June to August), sampled once a day (around 10:30 am) (as in Menon et al. (2008) for the 60°-70°N and 145°-165°W region for Sim PD and restrict our analyses to single-layer clouds with bases below 4 km and for similar optical depth and cloud droplet sizes as retrievals. Simulated average values for cloud thickness ranges from 100 to 900 m (average of 310 m) for CDNC, R_{eff}, LWP and COD are 60 cm^{-3}, 9.2 μm, 18 gm^{-2}, and 3.8, respectively. Although measurements were available at different time periods, and simulations were for a specific time period, differences between day

and night measurements were relatively small compared to seasonal differences [Zhao, personal communication].

For the Barrow region, for June to August for Year 1980 and 2000, DLW values of 320.3 and 331.3 Wm $^{-2}$ are obtained for the 60°-70°N and 145°-165°W region from retrievals described in Sec. 3.5.1. For Sim 1980 and PD, values of 303 Wm^{-2} were obtained and increases to 309.9 Wm^{-2} for 2030.

References

Albrecht B A 1989 *Science* **245**, 1227–1230.

Andreae M & Merlet P 2001 *Global Biogeochem. Cycles* **15**, 955–966.

Bell N, Koch D & Shindell D 2005 *J. Geophys. Res.* **110**, D14305,doi10.1029/2004JD005538.

Cao G, Zhang X & Zheng F 2006 *Atmos. Environ.* **40**, 6516–6527.

Chung C & Ramanathan V 2006 *J. Climate* **19**, 2036–2045.

Fernandes S, Trautmann N, Streets D, Roden C & Bond T 2007 *Global Biogeochem. Cycles* **21**, GB2019,doi:10.1029/2006GB002836.

Francis J 1997 *J. Geophys. Res.* **102**, 1795–1806.

Francis J & Hunter E 2007 *Envtl. Res. Lett.* **2**, doi:10.1088/1748–9326/2/4/045011.

Garrett T J & Zhao C 2006 *Nature* **440**, 787–789.

Hansen J, Sato M, Ruedy R, Nazarenko L & A. Lacis et al. 2005 *J. Geophys. Res.* **110**, doi:101029/2005JD005776.

He S & Carmichael G R 1999 *J. Geophys. Res.* **104**, 26307–26324.

Intergovernmental Panel on Climate Change 2007 *Climate Change 2007: The Physical Science Basis* Cambridge University Press. (S. Solomon, D. Qin, M. Manning, Z. Chen, M. Marquis, K.B. Averyt, M.Tignor and H.L. Miller, Eds.).

Kloster S, Dentener F, Feichter J, Raes F, van Aardenne J, Roeckner E, Lohmann U, Stier P & Swart R 2008 *Atmos. Chem. Phys.* **8**, 5563–5627.

Koch D, Bond T, Streets D & Unger N 2007a *Geophys. Res. Lett.* **34**. L05821,doi:10.1029/2006GL028360.

Koch D, Bond T, Streets D, Unger N & van der Werf G 2007b *J. Geophys. Res.* **112**. D02205,doi:10.1029/2005JD007024.

Koch D & Hansen J 2005 *J. Geophys. Res.* **110**, D04204,doi:10.1029/2004JD005296.

Lubin D & Vogelmann A M 2006 *Nature* **439**, 453–456.

Menon S & Del Genio A 2007 *Evaluating the impacts of carbonaceous aerosols on clouds and climate. In Human-induced climate change:An interdisciplinary assessment* Cambridge University Press. (M. Schlesinger et al., Eds.).

Menon S, Del Genio A, Kaufman Y, Bennartz R, Koch D, Loeb N & Orlikowski D 2008 *J. Geophys. Res.* . In Press.

Menon S, Hansen J, Nazarenko L & Luo Y 2002 *Science* **297**, 2250–2253.

Menon S & Rotstayn L 2006 *Clim. Dyn.* **27**, 345–356.

Ramanathan V, Chung C, Kim D, Bettge T, Buja L, Kiehl J T, Washington W M, Fu Q, Sikka D R & Wild M 2005 *Proc. Natl. Acad. Sci.* **102(15)**, 5326–5333.

Rayner N, Parker D E, Horton E B, Folland C K, Alexander L V, Rowell D P, Kent E C & Kaplan A 2000 *J. Geophys. Res.* **108(D14)**, 14891–14898.

Russell G, Miller J, Rind D, Ruedy R, Schmidt G & Sheth S 2003 *J. Geophys. Res.* **105**, 4407, doi:10.1029/2002JD002670.

Schmidt G A, Ruedy R, Hansen J E, Aleinov I & N. Bell et al. 2006 *J. Climate* **19**, 153–192.

Shindell D 2007 *Geophys. Res. Lett.* **34**, L14704,doi:10.1029/2007GL030221.

Shindell D, Faluvegi G, Aguilar N U E, Schmidt G, Koch D, Bauer S & Miller R 2006 *Atmos. Chem. Phys.* **6**, 4427–4459.

Shindell D, Faluvegi G, Bauer S, Koch D, Unger N, Menon S, Miller R, Schmidt G & Streets D 2007 *J. Geophys. Res.* **112**, D20103,doi:10.1029/2007JD008753.

Streets D 2005 *Asian Economic Papers* **4**, 1–23.

Streets D, Bond T, Lee T & Jang C 2004 *J. Geophys. Res.* **109**, D24212,doi:10.1029/2004JD004902.

Streets D, Wu Y & Chin M 2006 *Geophys. Res. Lett.* **33**, L15806,doi:10.1029/2006GL026471.

Twomey S 1991 *Atmos. Environ.* **25**, 2435–2442.

Unger N, Shindell D, Koch D, Amann M, Cofala J & Streets D 2006b *J. Geophys. Res.* **111**.

Unger N, Shindell D, Koch D & Streets D 2006a *Proc. Natl. Acad. Sci.* **103**, 4377–4380.

van der Werf G, Randerson J, Collatz G J, Giglio L, Kasibhatla P S, Arellano A F, Olsen S C & Kasischke E S 2004 *Science* **303**, 73–76.

Venkataraman C, Habib G, Eiguren-Fernandez A, A.H.Miguel & Friedlander S 2005 *Science* **307**, 1454–1456.

Yu H, Kaufman Y, Chin M, Feingold G & L.A. Remer et al. 2006 *Atmos. Chem. Phys. Discuss.* **5**, 7647–7768.

Zhao C & Garrett T J 2008 *J. Geophys. Res.* . "In review".

Table 1. Description of simulations used for the study. OM and BC refer to organic matter and black carbon, respectively. All simulations include interactive ozone chemistry coupled to the sulfate chemistry.

Simulation	Time Period	Aerosols and Processes treated
Sim 1980	1980	Sulfates, OM, BC and their Direct + Indirect effects
Sim PD	1995	Sulfates, OM, BC and their Direct + Indirect effects
Sim 2030	2030	Sulfates, OM, BC and their Direct + Indirect effects
Sim 2030A	2030	Similar to Sim 2030 but with 2x OM and BC from biofuel and transportation sources for Asia (10°S-40°N, 58°-122°E)
Sim 1980OS	1980	Sulfates and their Direct effect
Sim PDOS	1995	Sulfates and their Direct effect
Sim 2030OS	2030	Sulfates and their Direct effect

Table 2. Annual average instantaneous shortwave radiative forcings (Wm^{-2}) at the tropopause for the listed aerosol species for the three simulations. Values for ozone and the aerosol indirect effect include longwave forcings (Wm^{-2}). OM refers to organic matter, BCB to black carbon from biomass sources and BCF to black carbon from fossil- and biofuel sources.

Species	Sim 1980	Sim PD	Sim 2030	Sim PD-1980	Sim 2030-PD
Sulfate	-0.68	-0.64	-0.87	0.04	-0.23
OM	-0.17	-0.17	-0.15	0.00	0.02
BCB	0.15	0.15	0.13	0.00	-0.02
BCF	0.18	0.17	0.14	-0.01	-0.03
All Aerosols	-0.52	-0.49	-0.75	0.03	-0.26
Ozone	-0.37	-0.37	-0.25	0.00	0.12
Aerosol indirect effect	-30.57	-30.7	-31.38	-0.13	-0.68

Table 3. Radiative forcing efficiencies (Wg^{-1}) calculated from the ratio of direct forcing to column burdens for the listed aerosol species. OM refers to organic matter, BCB to black carbon from biomass sources and BCF to black carbon from fossil- and biofuel sources.

Species	Sim 1980	Sim PD	Sim 2030
Sulfate	-221	-230	-223
OM	-94.4	-94.4	-97.4
BCB	1071	1071	1083
BCF	1125	1063	1111

Table 4. Annual, June-July-August (JJA) and December-January-February (DJF) average values for TOA net radiation (NR-TOA), surface net radiation (NR-Sfc), shortwave and longwave cloud radiative forcing (SWCRF, LWCRF), aerosol direct forcing (DF) and ozone forcing (OF) at the tropopause, surface air temperature (SAT), water cloud cover (WCC), low cloud cover (LCC), total cloud cover (TCC) for the Arctic region (60°-90°N) for the three simulations.

Variable	Season	Sim 1980	Sim PD	Sim 2030	Sim PD-1980	Sim 2030-PD
NR-TOA	Annual	-102	-104	-104	-2.0	0.00
(Wm^{-2})	JJA	-3.93	-5.99	-3.26	-2.1	2.7
	DJF	-167	-169	-172.3	-2.0	-3.3
NR-Sfc	Annual	9.53	8.83	10.0	-0.70	1.2
(Wm^{-2})	JJA	76.9	74.8	79.3	-2.1	4.5
	DJF	-29.4	-29.5	-28.8	0.10	0.70
SWCRF	Annual	-17.5	-17.0	-17.9	0.50	-0.90
(Wm^{-2})	JJA	-49.3	-47.4	-50.4	1.9	-3.0
	DJF	-0.63	-0.64	-0.63	-0.01	0.01
LWCRF	Annual	16.9	17.4	18.0	0.50	0.60
(Wm^{-2})	JJA	22.3	22.1	22.4	-0.20	0.30
	DJF	11.2	12.6	13.0	1.4	0.40
DF	Annual	0.28	0.18	0.07	-0.10	-0.11
(Wm^{-2})	JJA	0.09	0.07	-0.11	-0.02	-0.18
	DJF	0.04	0.02	0.02	-0.02	0.00
OF	Annual	-0.12	-0.09	-0.11	0.03	-0.02
(Wm^{-2})	JJA	0.15	0.25	0.18	0.10	-0.07
	DJF	-0.24	-0.25	-0.26	-0.01	-0.01
SAT	Annual	-12.3	-11.1	-10.3	1.2	0.80
(C)	JJA	1.16	1.11	1.62	-0.05	0.51
	DJF	-24.0	-22.0	-20.2	2.0	1.8
WCC	Annual	16.5	16.9	18.8	0.40	1.9
(%)	JJA	40.5	40.1	43.8	-0.40	3.7
	DJF	2.61	3.28	4.07	0.67	0.79
LCC	Annual	81.2	81.0	80.0	-0.2	-1.0
(%)	JJA	71.4	71.3	69.6	-0.1	-1.7
	DJF	87.2	87.7	86.8	0.5	-0.9
TCC	Annual	86.1	86.0	85.5	-0.1	-0.5
(%)	JJA	79.9	79.8	78.8	-0.1	-1.0
	DJF	90.0	90.3	89.9	0.3	-0.4

Table 5. Annual average differences in ozone amount, aerosol surface mass, TOA net radiation (NR-TOA), surface net radiation (NR-Sfc), ozone forcing and aerosol forcing (aerosol direct + indirect effect) for the Asian region (10°S-40°N; 58° to 122°E) for the future cases.

Simulation	Ozone (ppbv)	Aerosol mass (μgm^{-3})	NR-TOA (Wm^{-2})	NR-Sfc (Wm^{-2})	Ozone forcing (Wm^{-2})	Aerosol forcing (Wm^{-2})
Sim 2030-PD	8.28	4.19	-2.5	-3.84	0.23	-0.86 (-0.50+ -0.36)
Sim 2030A-PD	8.35	13.61	-3.25	-3.58	0.25	-0.21(-0.48+ 0.27)

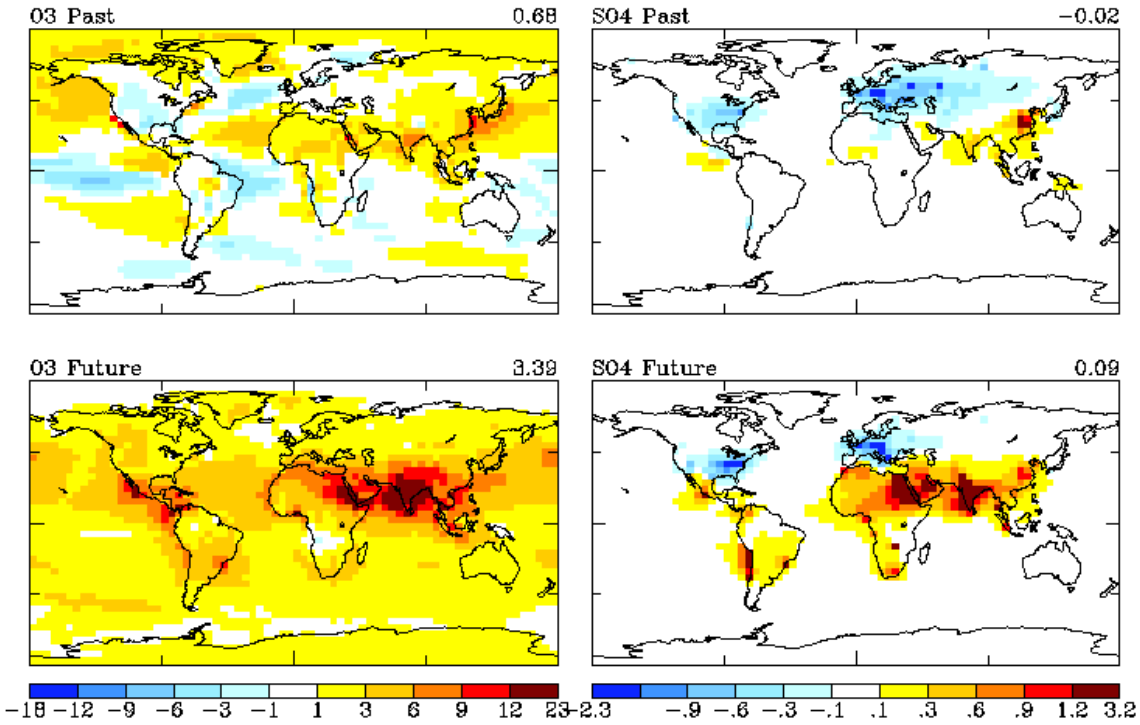

Figure 1. Average annual surface layer concentrations of ozone (O3) (ppbv) and sulfate (SO4) (μgm^{-3}) for the past (PD-1980) and future (2030 - PD).

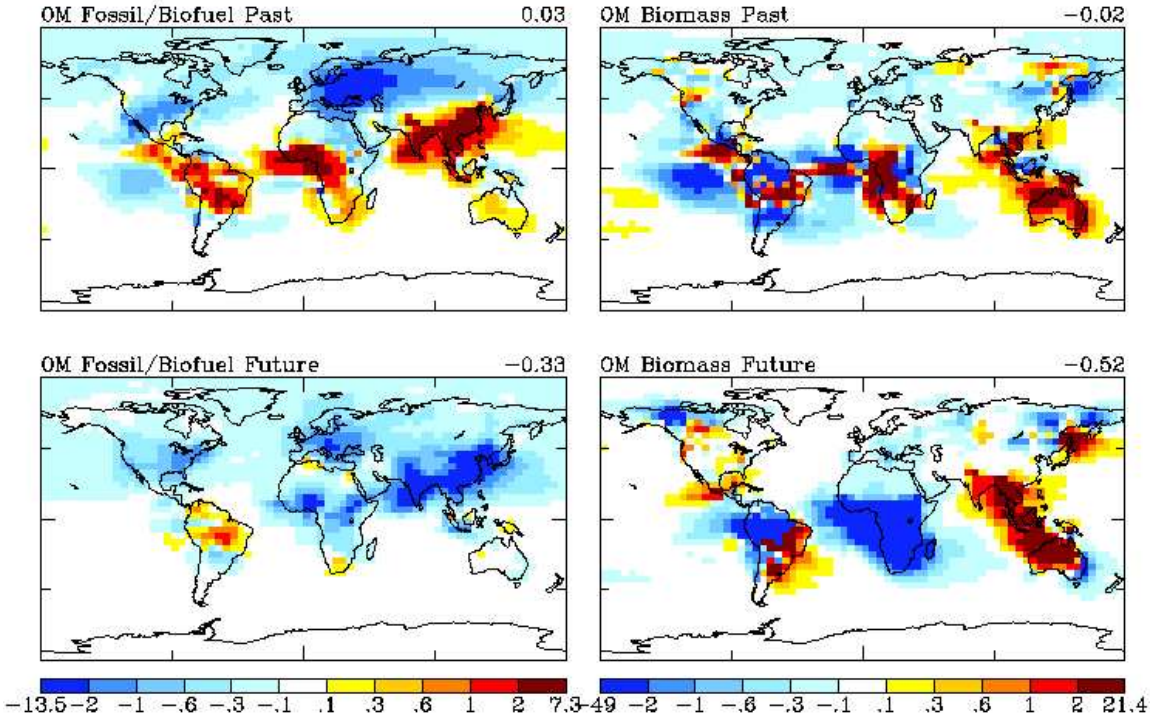

Figure 2. Similar to Fig. 1 but for organic matter (OM) (μgm^{-3}).

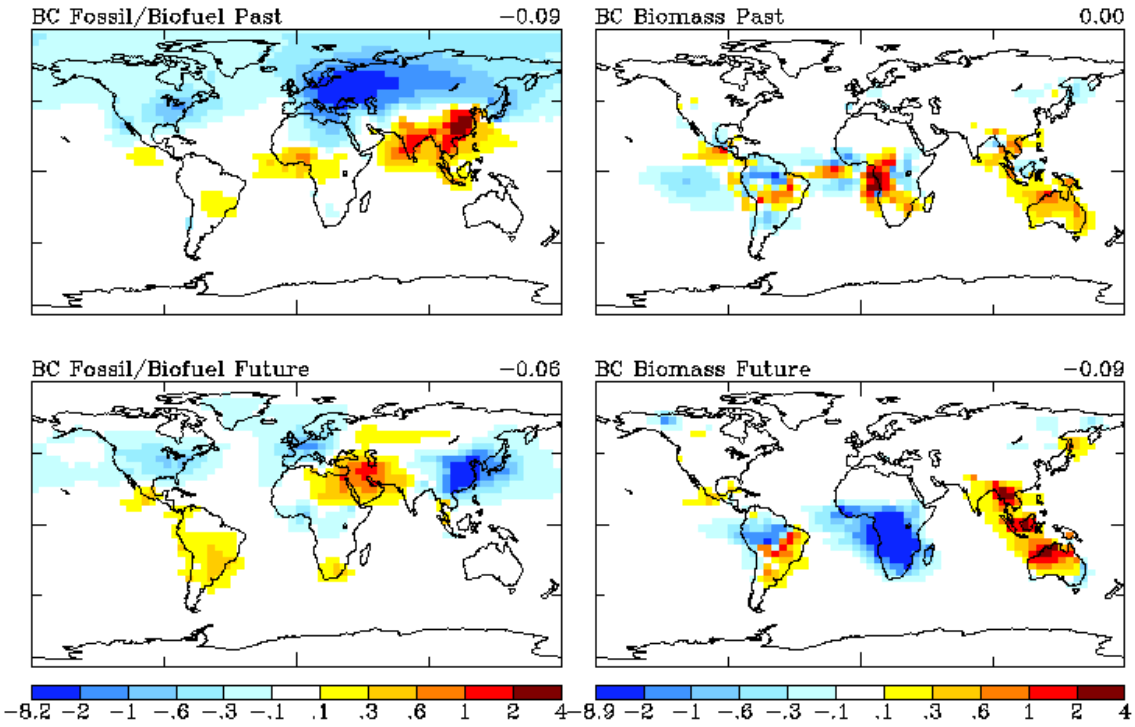

Figure 3. Similar to Fig. 2 but for black carbon (BC).

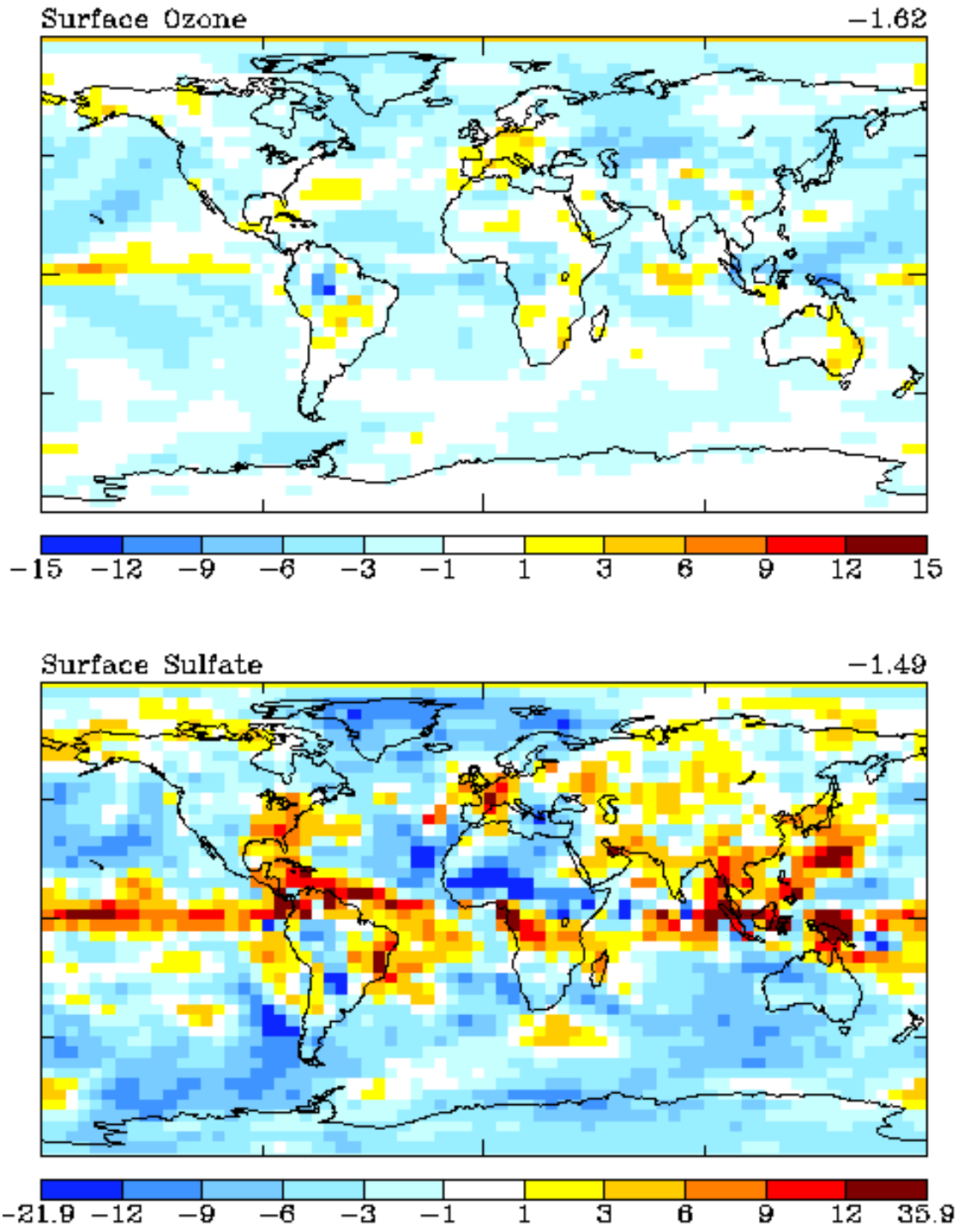

Figure 4. Percentage differences in surface ozone and sulfate concentrations between Sim 2030 and Sim 2030OS, given as (Sim 2030-Sim2030OS)/Sim2030OS.

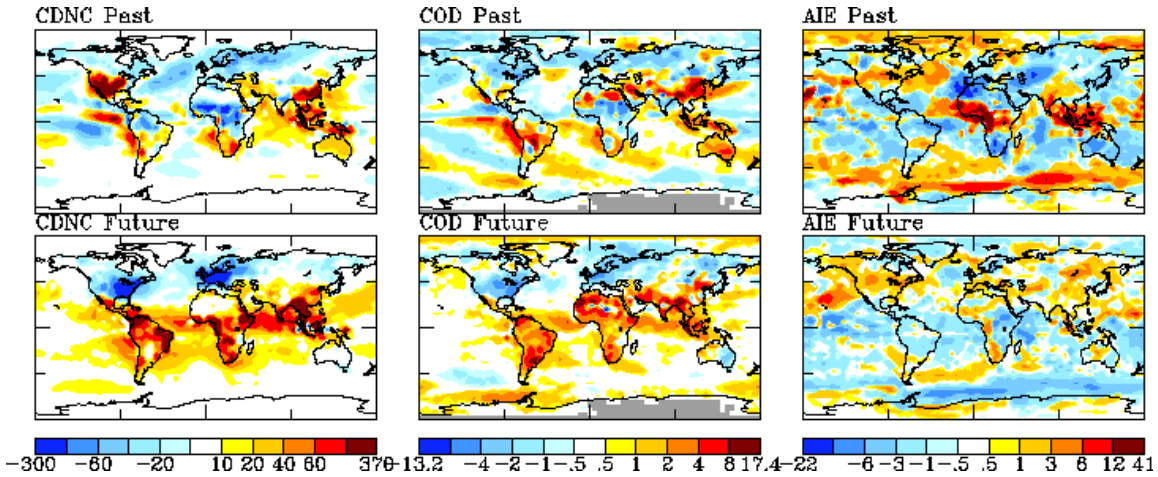

Figure 5. Global annual average cloud droplet number concentration (CDNC) in cm^{-3}, cloud optical depth (COD) and the aerosol indirect effects (AIE) in Wm^{-2} for the past (PD-1980) and future (2030-PD) cases.

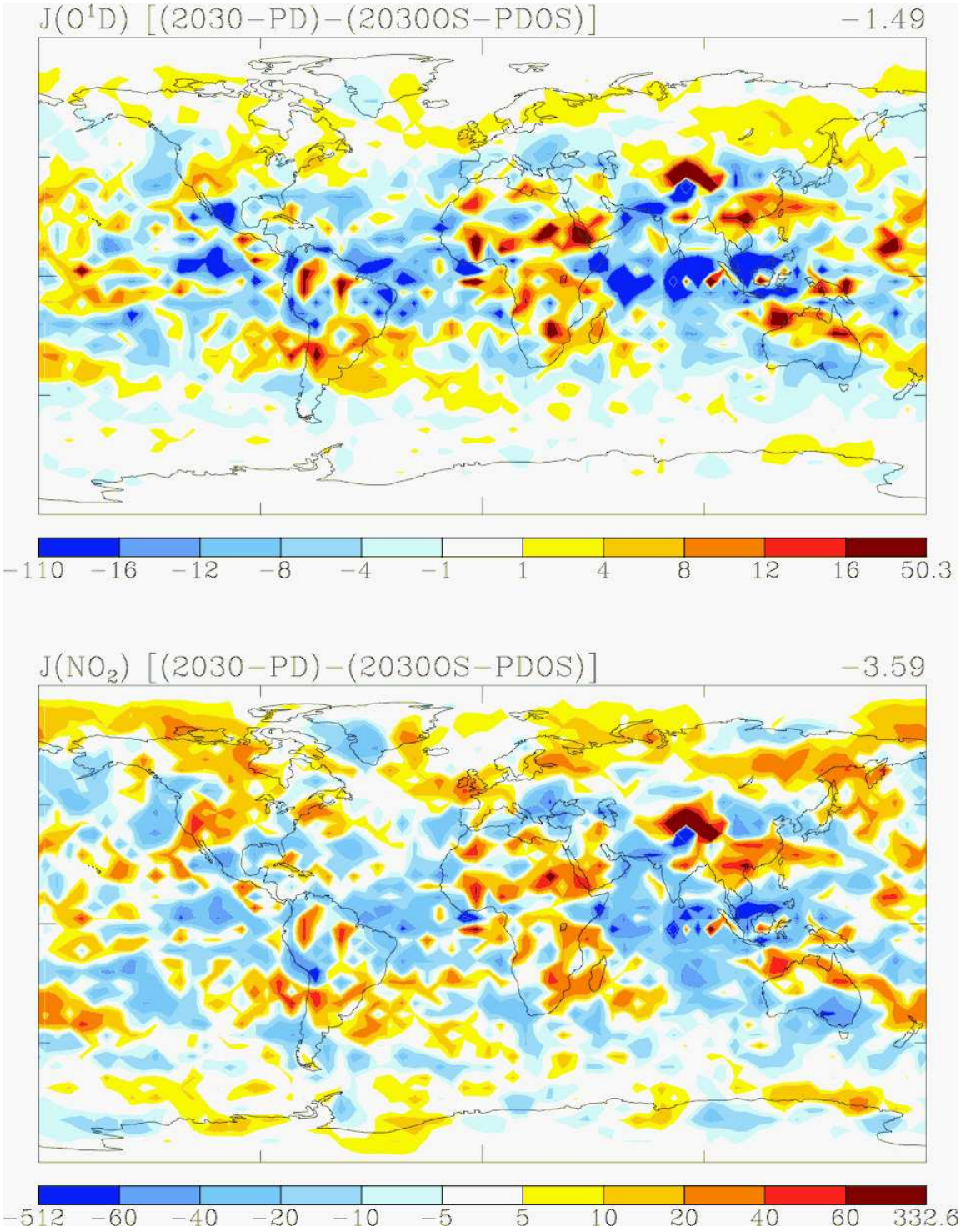

Figure 6. Impact of the aerosol indirect effect and carbonaceous aerosols on the change in annual average photolysis rates J(O1D) (top panel in 10^{-8} s^{-1}) and J(NO_2) (bottom panel in $10^{-6}s^{-1}$) between 2030 and 1995 [(2030-PD)-(2030OS-PDOS)].

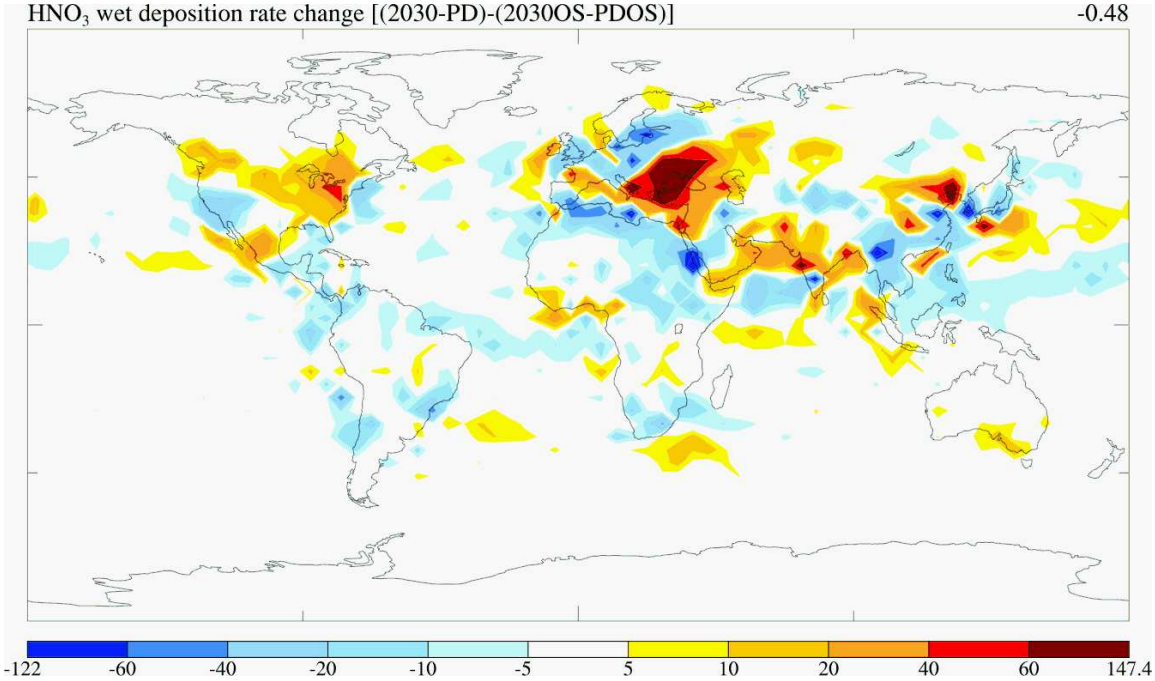

Figure 7. Impact of the aerosol indirect effect and carbonaceous aerosols on the change in annual average HNO_3 wet deposition rate (10^{-13} kg m^{-2} s^{-1}) between 2030 and 1995 [(2030-PD)-(2030OS-PDOS)].

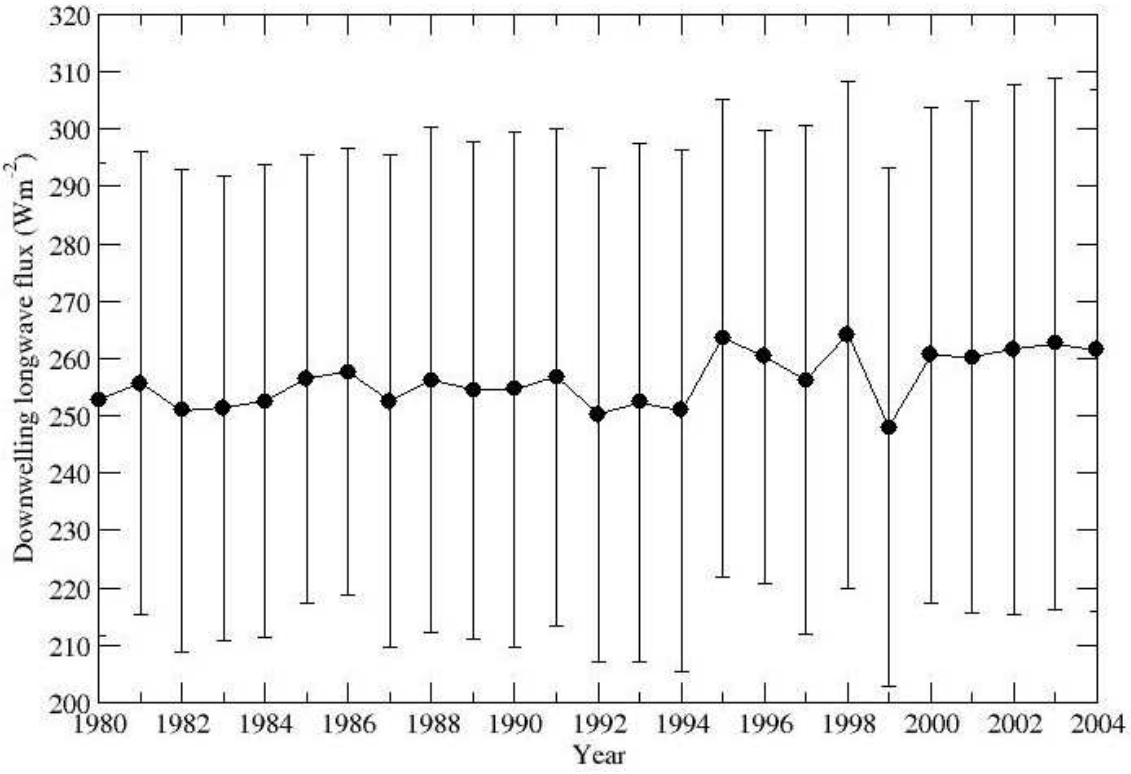

Figure 8. Annual averages of the downwelling longwave fluxes (Wm^{-2}) from 1980 to 2004 for the 60°-90°N region as obtained from TOVS retrievals by Francis (1997).

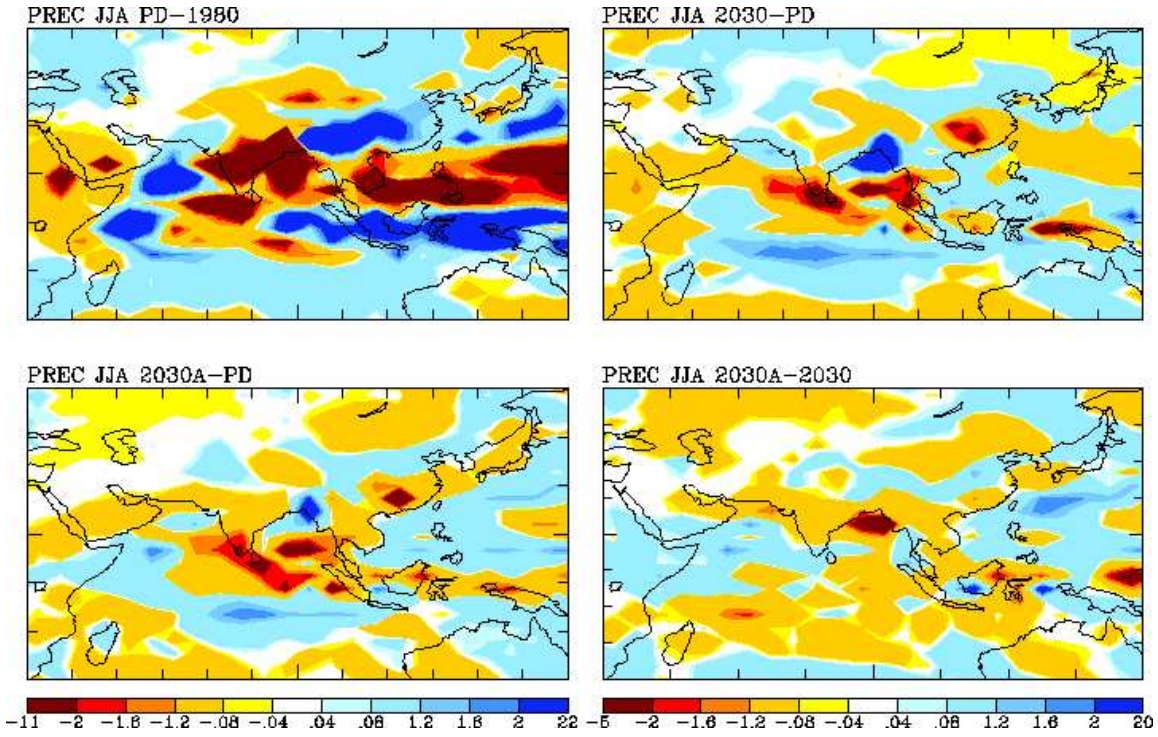

Figure 9. June-July-August (JJA) precipitation (PREC) (mm/day) differences between Sim PD and 1980; Sim 2030 and PD; Sim 2030A and PD; and Sim 2030A and 2030 for 30°S to 60°N and 30° to 150°E.